Contact damage in a Ce-TZP/Al$_2$O$_3$ nanocomposite

F.G. Marro [a,b,*], A. Mestra [a,b], M. Anglada [a,b]

[a] Department of Materials Science and Metallurgical Engineering, Universitat Politècnica de Catalunya, Av. Diagonal 647, 08028 Barcelona, Spain
[b] Center for Research in Nanoengineering, CRnE, Universitat Politècnica de Catalunya, Pascual i Vila 15, 08028 Barcelona, Spain

Abstract

The damage tolerance of a nanocomposite based on Ce-TZP and 30 vol% Al$_2$O$_3$ has been studied under monotonic contact with a spherical indenter. The results are compared with those previously known for commercial 3Y-TZP zirconia. It is concluded that the minimum load for ring crack appearance is similar in both ceramics. However, in the nanocomposite the ring cracks penetrate much less into the bulk, because of its higher fracture toughness. Finally, the stress-induced phase transformation of the zirconia component was quantified and mapped by micro-Raman spectroscopy.

1. Introduction

Tetragonal polycrystalline zirconia stabilized with 3 mol% of yttria (3Y-TZP) is a well known ceramic which possesses both a good biocompatibility and interesting mechanical properties, and it is currently being used in dental devices and implants.[1] On the other hand, it is known[2] that the surface of 3Y-TZP may suffer a transformation to monoclinic phase when exposed to humid environment. This spontaneous phase transformation is accompanied by micro-cracking and a loss of the mechanical properties in the affected surface. The phenomenon is often referred to as low temperature degradation (LTD) or hydrothermal ageing and is a serious drawback for the long-term stability and reliability of this ceramic.

There have been different approaches to develop ceramics resistant to LTD degradation while keeping a high mechanical strength. Most of them are based on ceria stabilized zirconia (Ce-TZP), magnesia partially stabilized zirconia (Mg-PSZ), or alumina–zirconia composites. Ce-TZP and Mg-PSZ exhibit higher resistance to LTD[3,4] as compared to 3Y-TZP, but their optimized strength is inferior. In Ce-TZP, this is

partly due to a larger grain size of about 0.8 μm as compared to the typical 0.3 μm grains of 3Y-TZP. Several attempts have been made on increasing the mechanical strength and LTD resistance of zirconia ceramics by adding alumina during the processing stage. Nawa and co-workers[5,6] developed in 1998 one such interesting nanocomposite containing Ce-TZP and 30 vol% alumina. The presence of alumina allows achieving a final average grain smaller than typical Ce-TZP. The resulting nanocomposite maintains thus a similar hardness and mechanical strength as biomedical grade 3Y-TZP, while it has both a much higher fracture toughness and resistance to LTD degradation.[7] More recently, new Ce-TZP/Al$_2$O$_3$ nanocomposites have been reported[8–10] with even a slightly higher strength than commercial 3Y-TZP zirconia.

Originally these nanocomposites were created with the purpose of replacing 3Y-TZP as a bearing material in hip joint replacements. Indeed, there are already some studies regarding to the tribological behaviour of these nanocomposites.[11,12] However, nowadays zirconia-based ceramics are gaining also substantial interest in the dental industry. In dental applications, the damage induced by contact loading is very important; however there is surprisingly a lack of information in this area. The present work focuses on the behaviour of a Ce-TZP/Al$_2$O$_3$ nanocomposite under the application of monotonic contact forces by means of spherical indentation. The objective was to determine the contact pressure necessary for the appearance of damage, and to compare the characteristics

of such damage with the known behaviour of standard 3Y-TZP.

2. Material and procedures

The nanocomposite was provided in the form of discs (diam. 50 mm, thickness 5 mm, Panasonic Electric Works). It is composed of 70 vol% Ce-TZP containing 10 mol% ceria, and 30 vol% Al_2O_3. The details of fabrication are described elsewhere.[5,6] The microstructure was characterized by scanning electron microscopy (SEM). The density, measured by Archimedes method, is 5.53 g/cm³ and the elastic modulus is 242 GPa, as determined by the impulse excitation technique (GrindoSonic MK5i). Therefore, the nanocomposite has a smaller density and larger elastic modulus than 3Y-TZP (typically ~6.1 g/cm³ and ~220 GPa). Such small differences between both types of ceramics are a consequence of the presence of alumina in the nanocomposite (alumina typically has an elastic modulus of ~400 GPa and a density of ~4 g/cm³). The hardness, measured with a 1 kg Vickers indentation, is HV1 = (11.0 ± 0.2) GPa. This value is similar to those reported in literature, and it is slightly smaller than for 3Y-TZP for which HV1 ≈ 12 GPa. The exact hardness of the Ce-TZP present in the nanocomposite is not known but that of pure 12Ce-TZP with larger grain size is close to 9 GPa.[3,4]

In order to determine the resistance to low temperature degradation, specimens were exposed during 55 h to 131 °C water vapour in an autoclave pressurized at 2 bars. The formation of monoclinic phase was evaluated by X-ray diffraction. This was performed in a diffractometer (Philips MRD) with Bragg–Brentano symmetric-geometry configuration and using Cu K_α (40 kV and 30 mA) radiation. X-ray diffraction spectra were obtained at scan steps of 10 s and a scan size of 0.017°. From the spectra, the monoclinic phase content was calculated by the method proposed by Toraya et al.[13]:

$$V_m = \frac{1.311 \left(I_m^{\bar{1}11} + I_m^{111} \right)}{1.311 \left(I_m^{\bar{1}11} + I_m^{111} \right) + I_t^{101}} \tag{1}$$

Here, I_t and I_m represent the integrated intensities of (1 1 1) tetragonal and of either ($\bar{1}$ 1 1) or (1 1 1) monoclinic peaks, respectively.

2.1. Fracture toughness

In an attempt to estimate the indentation fracture toughness, it was found that the length of the cracks emanating from Vickers imprints were very short, so the equations developed for estimating the indentation fracture toughness could not be applied. It was then recurred to report the extension of the indentation cracks under four point bending.[7] For doing so, prismatic bars were cut from the delivered discs with dimensions 45 mm in length, 4 mm width and 5 mm in thickness. For each bar, the prospective tensile face was polished to mirror-like finishing and then indented with a 30 kg load with a Vickers indenter. The indenter was oriented in such a way that one of the imprint

diagonals was perpendicular to the specimen length. Finally, this indented specimen was tested by flexure in a four-point bending device with an external span of 20 mm and an internal span of 10 mm in a universal testing machine Instron 8511. The load was applied at increasing steps at a rate of 100 N/s and the crack growth was monitored after each increase in load by examining the tensile surface in a laser scanning confocal microscope (LSCM, Olympus Lext). In the presence of an applied stress, σ_{app}, parallel to the surface and perpendicular to one of the imprint diagonals (like in the present flexural test) the applied stress-intensity factor was estimated in the following way:

$$K_{app} = \psi \sigma_{app} \sqrt{c} \tag{2}$$

where c is the distance between the crack tip and the indentation centre, and ψ is a geometrical factor taken here as 1.29 which corresponds to a semicircular surface crack. This equation assumes that the cracks are connected below the indentation imprint. For Y-TZP, it is known that the indentation cracks are initially of Palmqvist type for the load considered here, however as the cracks grow during the test they will eventually connect below the imprint.

Finally, in order to remove all residual stresses from the indentation and from transformation, some specimens were annealed at 1200 °C during 1 h previous to the flexural test (a thermal treatment at this temperature is known to remove the residual stresses in zirconia ceramics[14]).

2.2. Spherical indentation

The response and tolerance of the nanocomposite to monotonic contact forces, was assessed by spherical indentation tests performed on the same testing machine Instron 8511 using 2.5 mm diameter WC balls as the indenters. This ball size was chosen as an optimum diameter for evaluating this nanocomposite based on previous studies in 3Y-TZP zirconia.[15] In spherical indentation, the produced deformation is usually defined as the ratio between the contact radius and the indenter radius, a/R. According to basic Hertzian theory,[16] the contact is initially in elastic regime and the mean pressure increases linearly with the deformation by indentation a/R:

$$p_0 = \left(\frac{4E_{eff}}{3\pi} \right) \frac{a}{R} \tag{3}$$

Here, the mean pressure is defined as $p_0 = P/\pi a^2$ (P being the contact load) and E_{eff} is the effective elastic modulus which is obtained from the elastic modulus of the sample (E) and the indenter (E') and from their Poisson coefficients (ν, ν'):

$$\frac{1}{E_{eff}} = \frac{(1 - \nu^2)}{E} + \frac{(1 - \nu'^2)}{E'} \tag{4}$$

On the other hand, during the plastic regime of the spherical indentation the empirical law of Meyer[17] is verified which can be expressed as:

$$p_0 = \Lambda \left(\frac{a}{R} \right)^{n-2} \tag{5}$$

Here, Λ and n are particular parameters associated only to the material. In particular, n usually takes a value in the range $2 \leq n \leq 2.5$. This law implies that, like in the elastic regime, also in the plastic regime the mean pressure is only a function of the deformation by indentation a/R. These tests are based on the evaluation of the residual imprint diameter, which is taken as an approximation of the maximum contact area during indentation. This technique has therefore some limitations to determine the contact area in the elastic regime (where there are no residual imprints). In order to dispose of additional data in this initial regime, nanoindentation was performed with a XP Nanoindenter using a spherical diamond tip of 54 μm of diameter. The system used has a continuous stiffness measurement modulus. The technique to obtain the contact area from a spherical nanoindentation test is already described in the literature.[18] Basically, from the constant stiffness measurement (S), the actual contact depth of the nanoindentation can be obtained with the method of Oliver and Pharr[19]:

$$h_c = h - \varepsilon \frac{P}{S} \qquad (6)$$

where h is the total displacement, P is the applied load and ε is a constant based on the indenter geometry ($\varepsilon = 3/4$ for a sphere). For a given test, the parameters h, P and S are known directly from the basic output of the equipment. Once the contact depth h_c is thus calculated for a spherical nanoindentation test, the contact radius can be calculated as follows:

$$a^* = \sqrt{2h_c R^* - h_c^2} \qquad (7)$$

where R^* is the radius of the sphere. Using this technique, the actual contact radius can be obtained from the basic data of a nanoindentation test; then the applied contact pressure and the deformation can be finally obtained. By plotting these last parameters, a stress/deformation curve for each spherical nanoindentation test can be drawn. In the present case, such a curve was obtained by averaging the results of several tests. Some of the imprints produced by these tests on the surface of polished specimens were later visualized by atomic force microscopy (AFM, Veeco Dimension) in tapping mode.

The phase-transformation mechanism of the Ce-TZP zirconia component was assessed by micro-Raman spectroscopy on some of the residual imprints produced by spherical indentation. Spectra were collected with a triple monochromator spectrometer T64000 (Horiba/Jobin-Yvon) with a coupled CCD detector cooled with liquid nitrogen. The source of excitation was an Argon-ion laser Innova 300 (Coherent Laser Group) at 514 nm wavelength. The spectrum integration time was 60 s with averaging the recorded spectra over two successive measurements. The laser beam was focused using an optical microscope with 100× long-focal objective (lateral resolution of ~1 μm) while a monitor screen connected to the microscope allowed exploring the sample and recording the spectra from the surface on the residual imprints. For all spectra, a linear subtraction of the background was made, and the integrated intensity bands were

calculated. From the spectra, the monoclinic volume fraction was estimated as follows[20,21]:

$$V_m = \frac{I_m^{181} + I_m^{190}}{2.2I_t^{147} + I_m^{181} + I_m^{190}} \qquad (8)$$

Here, I_m and I_t represent the integrated intensities of the monoclinic and tetragonal peaks, respectively; the super-indexes identify the Raman shift in cm^{-1} units.

3. Results

3.1. Microstructure and resistance to LTD

The microstructure of the nanocomposite consisted of two constituents, Ce-TZP and Al_2O_3, which can be appreciated respectively as clear and dark grains as observed by SEM microscopy (Fig. 1). The zirconia grains, though still submicrometric, are larger than the alumina grains. It was found that the Al_2O_3 grains had an average size of (0.38 ± 0.11) μm, while for Ce-TZP it was (0.56 ± 0.20) μm. According to Nawa et al.,[5] who have completely characterized the microstructure, it is formed by an interpenetrated intragranular nanostructure in which either nanometer-sized Ce-TZP or Al_2O_3 particles are located within submicron-sized Al_2O_3 or Ce-TZP grains, respectively.

From the X-ray diffraction analysis, it was found a very small formation of monoclinic content of less than 5 vol% in the zirconia constituent after hydrothermal exposure (Fig. 2). This fraction of monoclinic phase is much smaller than the one found[22,23] in 3Y-TZP under identical conditions of hydrothermal ageing (about 50 vol%).

3.2. Fracture toughness

For 3Y-TZP, it is common to report the fracture toughness from the length of the cracks induced by Vickers indentation. For the present nanocomposite, such an indentation does not produce cracks long enough for making this estimation (Fig. 3), since the cracks are too short to apply equations of indentation fracture toughness or even difficult to observe at the vertices of the imprint. The situation is similar to that found in very
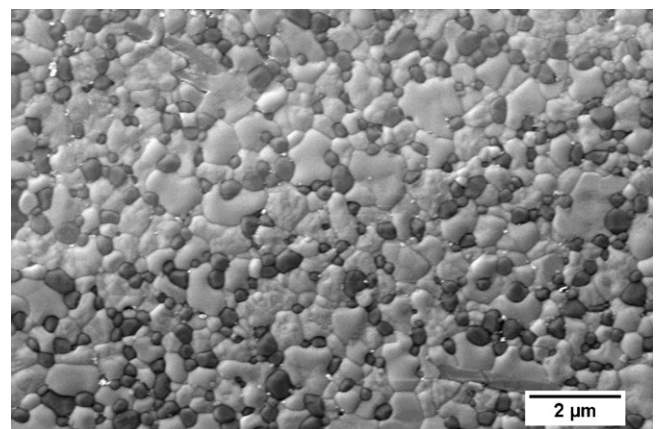
Fig. 1. Scanning electron micrograph of the Ce-TZP/Al_2O_3 nanocomposite, showing both the zirconia (clear grains) and alumina.
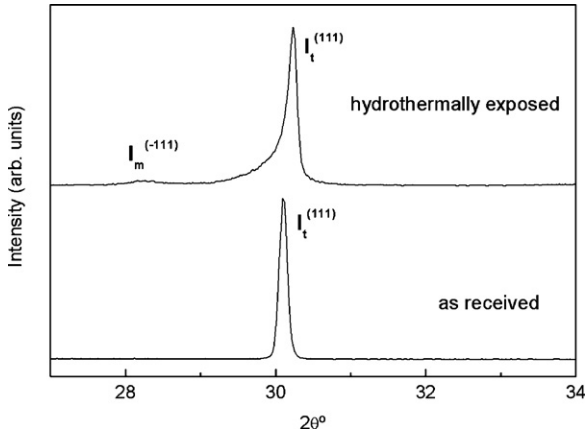
Fig. 2. X-ray diffraction patterns: (bottom) as received nanocomposite, (top) after hydrothermal exposure. The peaks with labels correspond to the monoclinic and tetragonal phases of the zirconia phase.

tough zirconia ceramics of high transformability. In this sense, the situation is very different from 3Y-TZP of biomedical grade for which cracks are long so that the effect of transformation in the neighbourhood of the indent is very restricted and has not a strong effect on the crack length.

In order to estimate the fracture toughness, indented prismatic specimens were subjected to four point bending and the crack growth was monitored as the load was incremented (see Section 2). In theory, the total stress intensity factor during such a test should include not only the applied stress intensity factor K_{app} (see Eq. (2)) but also a residual stress intensity factor K_{res}. This additional factor is related to the residual stresses induced by the indentation, which act opening the crack. Together with these contributions (K_{app} and K_{res}), it should be considered also the relevant phase transformation which occurs close to the vertices of the indentation imprints and generates a compressive stress on the crack flanks in this region. This stress has an effect on the crack tip which is very important when the crack is short and will be represented as a negative contribution K_{transf}.

In principle it would be possible to remove both factors (K_{res} and K_{transf}) by annealing the indented specimen and observing the crack extension under four point bending. In order to simplify the analysis of the data, one test was performed where the specimen had been previously annealed to remove these residual stresses. Fig. 4(a) shows the increase of K_{app} with the crack growth in this case. Although there is a substantial scatter of data, K_{app} was seen to increase up to 10.7 MPam$^{1/2}$ before final fracture.

It is also possible to analyze these crack propagation tests when the specimen has not been annealed and retains the residual stresses from the indentation. Benzaid et al.[7] performed one such test on a similar nanocomposite, showing that it is interesting to
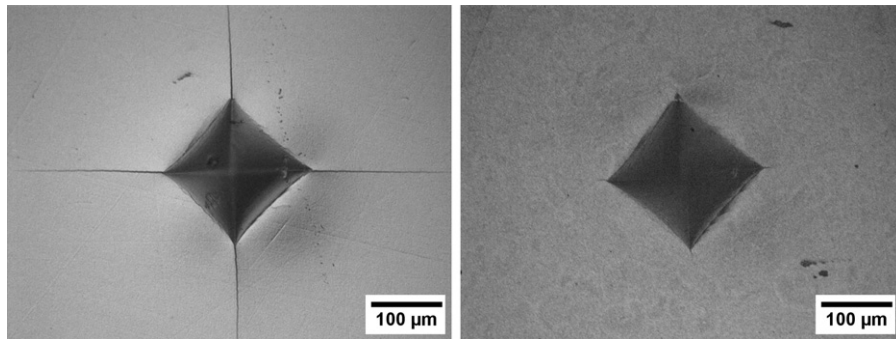
Fig. 3. Vickers indentation with a 30 kg load: (left) as sintered 3Y-TZP zirconia, (right) as received Ce-TZP/Al$_2$O$_3$ nanocomposite.
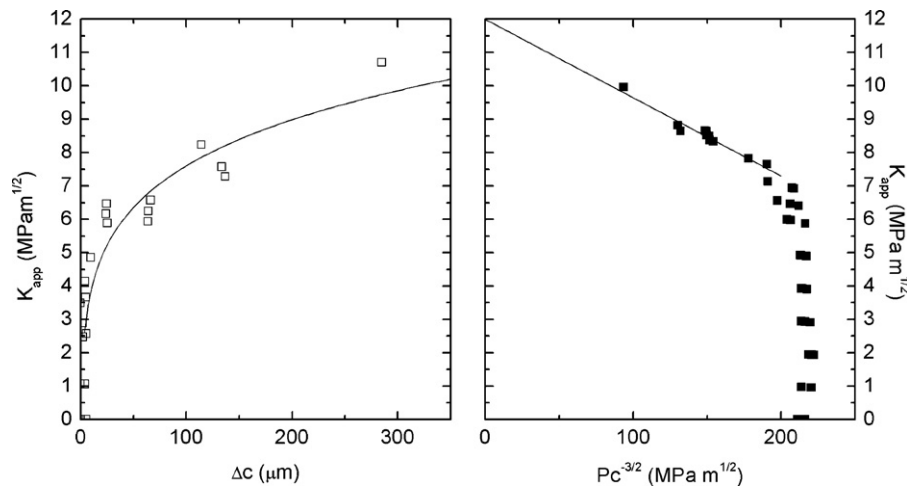
Fig. 4. Applied stress-intensity factor determined for indentation cracks subjected to flexural tests: (a) increase of K_{app} with the crack growth for a specimen previously annealed, (b) representation of K_{app} versus $P/c^{-3/2}$ in a test where the specimen has not been annealed (methodology similar to the one reported by Benzaid et al.[7]).
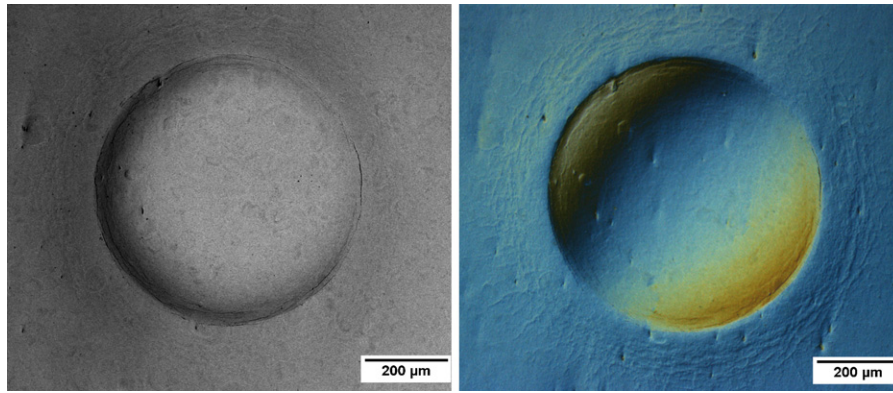
Fig. 5. Residual imprint for a 3500 N load: (left) LSCM image; (right) Nomarski interferometry.

represent K_{app} against $P/c^{3/2}$ (where P represents the indentation load). This representation shows a linear dependence when the cracks propagate, and the fracture toughness was estimated by those authors by the extrapolation of the linear behaviour giving 9.7 MPam$^{1/2}$. In the present work, one such test was performed also in a specimen that had not been annealed. From the K_{app} against $P/c^{3/2}$ representation of this test (Fig. 4(b)), the fracture toughness of the nanocomposite is estimated approximately as 12.0 MPam$^{1/2}$. Comparing the results of both methodologies performed (Fig. 4(a)–(b)), it seems that the fracture toughness of the nanocomposite is in the range (11 ± 1) MPam$^{1/2}$. This is slightly larger than the previously mentioned value of Benzaid et al., probably due to the fact that the present nanocomposite has a coarser microstructure (average grain size is 0.48 μm as compared to 0.25 μm for the nanocomposite of Benzaid et al.).

3.3. Monotonic contact damage

Regarding to the monotonic contact behaviour of the nanocomposite, the radius of the residual imprint was measured and the mean pressure and the deformation by indentation a/R was obtained for the different applied loads. Below an indentation load of 200 N, no residual imprint could be observed, indicating that the applied mean pressure below this limit approximately corresponds to the elastic regime. Imprints became visible above this load. Even for the smallest imprints, it was possible to appreciate some kind of deformation around the imprint border. This was especially noticeable when observing the imprint by Nomarski interferometry (Fig. 5). This roughness around the imprint is caused by tetragonal–monoclinic

phase transformation of the Ce-TZP present in the nanocomposite. Actually, the formation of autocatalytic transformation bands on a tensile surface is typical of pure Ce-TZP.[24] Therefore, the transformation observed around the imprint is not surprising considering that the contact border is the location where theoretically[16] the tensile stress is maximum in the elastic regime.

Damage was first detected for a load of 1500 N in the form of a ring crack. This minimum load for ring cracking is similar to that observed previously[15] on 3Y-TZP using exactly the same test. For a load higher than 2000 N, secondary rings begin to appear, and above 3000 N several secondary rings had already formed.

In order to observe the extension of the ring cracks inside the bulk, the imprint produced by the highest applied load (4000 N) was considered. For this high load, several successive ring cracks had already formed inside the imprint (Fig. 6). A cross-section of this indentation was cut and polished with colloidal silica in an effort to observe possible cone cracks. These cracks are typical of this type of indentation on brittle materials like ceramics.[15,16] Close observation at the border showed that the ring cracks penetrate only very few microns into the bulk. This is relevant since well developed longer cone cracks are clearly visible in 3Y-TZP in similar previous tests.[15] Therefore, the present results indicate that the Ce-TZP/Al$_2$O$_3$ nanocomposite has a higher resistance for ring cracks propagating inside the bulk than 3Y-TZP, probably due to its higher fracture toughness.

From the permanent spherical indentation imprints, the stress–strain deformation curve was obtained (Fig. 7). The smallest applied load for which permanent deformation was
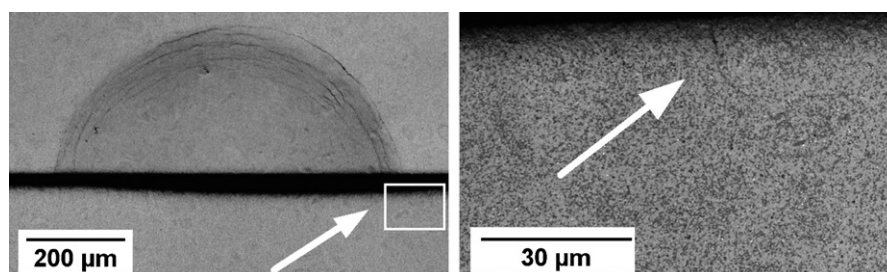
Fig. 6. LSCM image of a 4000 N spherical imprint: (left) surface and polished cross-section; (right) zoom of a ring crack in the cross-section.
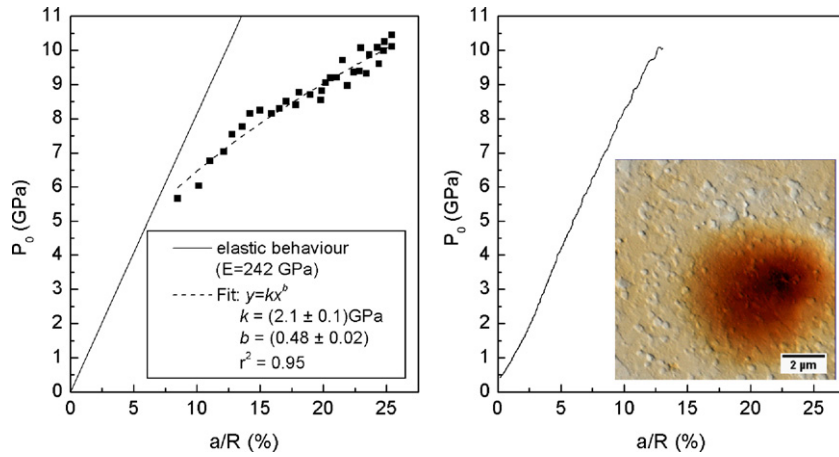
Fig. 7. (Left) Indentation stress–strain curve obtained from the monotonic contact tests; also shown are the theoretical elastic regime calculated from the Young modulus of the material (solid line) and the fit of the data to Meyer's law (dashed line, see Eq. (5)). (Right) Indentation stress–strain curve as obtained by spherical nanoindentation in the elastic regime. The inset image corresponds to a micrograph of a nanoindentation imprint seen by atomic force microscopy (AFM).

detected (200 N) corresponds to an applied mean stress of 5.9 GPa. At higher loads, the maximum applied mean stress increases by increasing the load until around 10 GPa, where the increase in pressure becomes slower as the value of hardness for the material is approached. The fitting of the data to the Meyer's law (Eq. (5)), yields a parameter $n = 2.48 \pm 0.02$ for the present nanocomposite.

In order to determine the part of the indentation stress–stain curve that remains in elastic regime, the technique of spherical nanoindentation was considered (see experimental procedure). The obtained data (Fig. 7) shows effectively how this section of the curve approaches the theoretical elastic regime (Eq. (3)).

3.4. Stress-induced phase transformation

Because in the nanocomposite the volume fraction of Ce-TZP is large and it is highly transformable, monoclinic phase may be produced locally when a contact load is applied. This stress-induced transformation was evaluated by micro-Raman spectroscopy in the 3500 N imprint. Spectra were taken along the diameter of the imprint and around the border. Most mon-

oclinic phase was produced at the border of the deformation circle (Fig. 8). At this location, the estimated local monoclinic content is 25%, while at the centre of the circle was less than 5%. This is not surprising considering the stress distribution induced by the spherical indentation, which has a tensile component at the border, but in the centre of the contact the stresses are compressive.

Phase transformation is then the mechanism by which the nanocomposite is more tolerant to deformation without producing deep cone cracks as in 3Y-TZP. This mechanism plays also an important role in the fracture toughness of the nanocomposite. Although it is well known that Ce-TZP has large fracture toughness in the form of an isolated single phase with a large grain size, here it is shown that even by reducing the grain size of Ce-TZP and in the presence of the constraint to deformation by the alumina phase, transformability is still higher than for 3Y-TZP with a similar grain size. Despite this stress-activated high transformability, the nanocomposite has good resistance to LTD, since, after 30 h of hydrothermal ageing, the amount of monoclinic phase detected on the surface was very low. This makes an important difference with 3Y-TZP, since although the
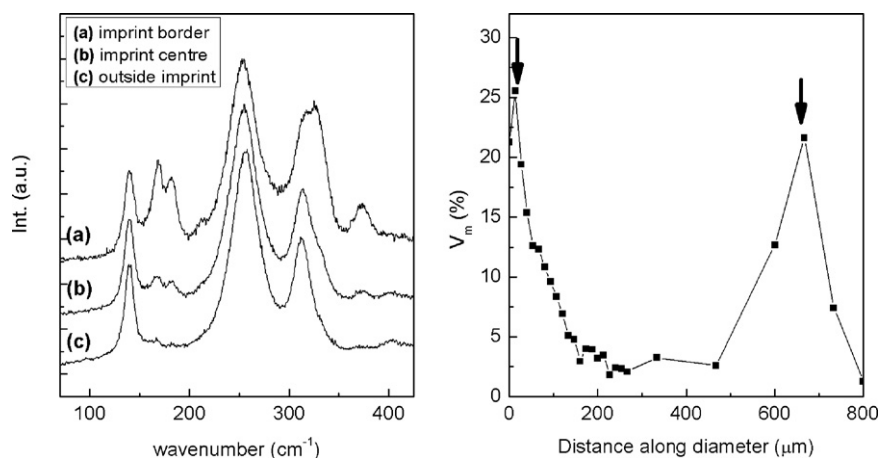
Fig. 8. (Left) Raman spectra on different zones of a residual imprint produced by a 3500 N spherical indentation, (right) obtained monoclinic content across the imprint diameter (arrows indicate the position of imprint borders).
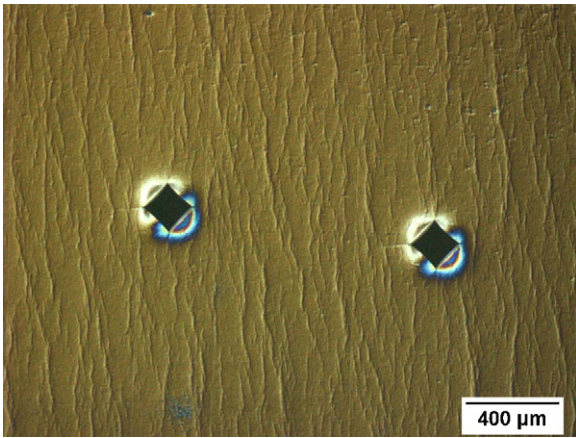
Fig. 9. Surface of a prismatic specimen after bending (image taken with Nomarski interferometry). Under this flexion test, longitudinal bands began to appear perpendicular to the applied stress (in this picture, the applied stress corresponds to the horizontal direction).

latter can be made more transformable by increasing the grain size, this is inevitably accompanied by a much lower resistance to low temperature degradation. It should be remembered also that the transformation toughening mechanism is based on the volumetric expansion of the Ce-TZP component when it transforms to monoclinic phase under the presence of an applied external stress. Additionally, it is relevant to remember also that this nanocomposite is reported to present nanoinclusions of one component inside the other,[5] which provide a further toughening mechanism.

The high transformability of the nanocomposite can also be appreciated by the roughness that appears in the form of bands in a direction perpendicular to the applied stress. To observe better these bands, a prismatic rectangular bar was cut and machined from the supplied discs. One of its longitudinal faces was polished with 3 µm diamond paste, and then further up to colloidal silica to achieve mirror-like finishing. The surface of this specimen was then subjected to four-point bending until fracture with the polished surface in the tensile face. This surface, with several indentations used for marking, was observed by Nomarski interferometry (Fig. 9), showing that catalytic bands were formed prior to fracture.

4. Discussion

When considering indentation cracks for the evaluation of the fracture toughness, it is necessary to take into account the different contributions to the total stress intensity factor at the crack tip K_{tip}. If the indentation crack is employed in a flexural test, K_{tip} will correspond to the applied external stress intensity factor K_{app} and also a factor K_{res} accounting for the indentation residual stresses. In principle, these residual stresses can be eliminated with an appropriated annealing treatment of the sample. On the other hand, compressive stresses may be also present along the indentation crack as a consequence of a volume expansion of the material near the vertices of the imprint. Indeed, we believe this is the case for the present nanocomposite. This material presents an important pile-up zone around the imprint which has an effect of closing the crack. This is a consequence of the phase-transformation of the Ce-TZP component present in the material. In this case, the total stress intensity factor of a non-annealed indentation crack which is tested to an external stress adopts the following expression:

$$K_{tip} = K_{app} + K_{res} + K_{transf} \qquad (9)$$

Here, K_{transf} accounts for the stresses due to the transformation of the material around the crack. In order to understand the effect of these stresses in an indentation crack, it will be discussed here a simple one-dimensional model. In this model, the coordinate x represents the distance from the imprint centre (see Fig. 10). Along this dimension, a function $P(x)$ is considered which corresponds to transformation stresses per unit of length induced by the imprint which act near the vertices of the imprint and which tend to close the crack. The total stress intensity factor for a crack of dimension c under stress distribution equal to $P(x)$ can be computed in the following way[25]:

$$K_{transf} = \frac{1}{\sqrt{\pi c}} \int_{-c}^{c} P(x) \sqrt{\frac{c+x}{c-x}} dx \qquad (10)$$

Assuming that the transformation stress distribution is constant ($P(x) = -P$) over a range $\{-(a+t) \leq x \leq -a; a \leq x \leq a+t\}$ which represents the residual compressive stress region; and $P(x) = 0$ outside this range, then the integration of equation 10
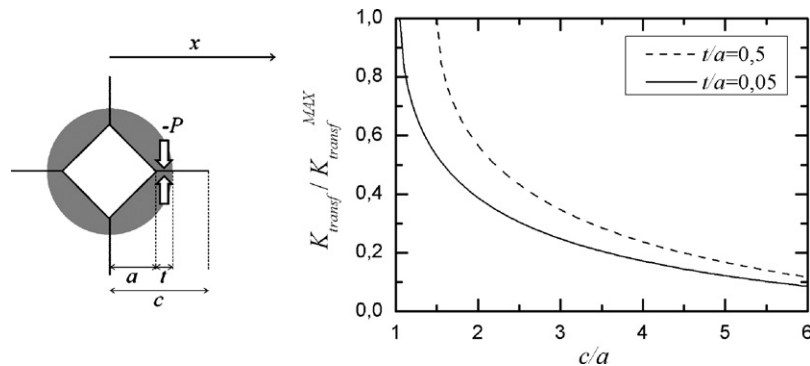
Fig. 10. Stresses due to volume expansion of the material surrounding an indentation crack: (left) Schematic representation of the compressive region around the imprint; (right) relative dependence of the stress-intensity factor K_{transf} with the crack length; two sizes (t/a) of the compressive region are considered for the calculation (see Eq. (11)).

yields the following expression:

$$K_{transf}\left(\frac{c}{a}\right) = -2P\left(\frac{a}{\pi}\right)^{1/2}\left(\frac{c}{a}\right)^{1/2}$$
$$\times\left[\arcsin\left(\frac{a}{c}\left(1+\frac{t}{a}\right)\right) - \arcsin\left(\frac{a}{c}\right)\right] \quad (11)$$

This expression represents the transformation stress intensity factor as a function of the relative crack length c/a. This solution is valid only for $c \geq (a+t)$; i.e. when the crack is larger than the compressive region. The absolute value of the transformation stress intensity factor is maximum $(|K_{trans}|^{MAX})$ when the crack is smallest. It is possible then to represent the relative dependence of K_{transf} with the crack length (see Fig. 10).

For Ce-TZP/Al$_2$O$_3$ nanocomposites, it has often been reported that the indentation fracture (IM) method overestimates the real fracture toughness. In the present nanocomposite, the IM method yielded a value of around 20 MPam$^{1/2}$; while it became obvious from the described flexural tests that a value of 10 MPam$^{1/2}$ was much more realistic. This would imply that, just after indentation, the compressive stresses are very important (i.e. the crack remains inside the compressive region) and K_{transf} can reach high values which could account for the large toughness found by indentation fracture toughness. Considering then Fig. 10, this means that even for long indentation cracks, K_{transf} can still contribute significantly to fracture toughness. This is probably the reason for the highest fracture toughness measured in the non-annealed specimens with respect to the only indented specimens.

Regarding to the monotonic contact damage studied, the largest cone cracks produced by the spherical indentation tests did not penetrate more than about 15 μm into the bulk. The nanocomposite is reported to have a flexural strength of about 1000 MPa; i.e. similar to 3Y-TZP (actually, this was further corroborated here by biaxial flexure tests). This strength corresponds to approximately a critical defect size of 17 μm. This implies that the monotonic contact tests induced here do not produce defects larger than the critical crack size of the material. This is relevant since, in 3Y-TZP of similar strength,[15] larger cone cracks are reported. This would imply that the mechanical strength of the present nanocomposite is less affected by contact damage than commercial 3Y-TZP.

5. Conclusions

The tolerance of a Ce-TZP/Al$_2$O$_3$ nanocomposite to monotonic contact was evaluated by spherical indentation. These tests were performed in order to understand the viability of this new type of ceramic in medical applications like dental prosthesis, and to compare it to existing data on biomedical grade 3Y-TZP zirconia. The minimum load for the appearance of damage was found to be similar to standard 3Y-TZP evaluated with the same methods. However, in the nanocomposite the induced cracks propagate less into the bulk material due to its high fracture toughness; which is caused by the high tetragonal-to-monoclinic (t–m) transformability of the Ce-TZP component. The damage produced, even by the highest load, was smaller than the nat-ural critical defect size of the nanocomposite. This suggests that even the most severe Hertzian monotonic load used here, would not affect its mechanical strength. The stress-induced phase transformation of the Ce-TZP component was mapped all over the imprint produced by the spherical contact, showing that the transformation is maximal at the border. Finally, in spite of the high t–m transformability, the nanocomposite is also more resistant to low temperature degradation than standard 3Y-TZP.

References

1. Denry I, Kelly R. State of the art of zirconia for dental applications. *Dent Mater* 2008;**24**:299–307.
2. Kobayashi K, Kuwajima H, Masaki T. Phase change and mechanical properties of ZrO$_2$–Y$_2$O$_3$ solid electrolyte after ageing. *Solid State Ionics* 1981;**3–4**:489–93.
3. Tsukuma K. Mechanical properties and thermal stability of CeO$_2$ containing tetragonal zirconia polycrystals. *Am Ceram Soc Bull* 1986;**65**:1386–9.
4. Tsukuma K, Shimada M. Strength, fracture toughness and Vickers hardness of CeO$_2$-stabilized tetragonal ZrO$_2$ polycrystals. *J Mater Sci* 1985;**20**:1178–84.
5. Nawa M, Bamba N, Sekino T, Niihara K. The effect of TiO$_2$ addition on strength and toughening in intragranular type 12Ce-TZP/Al$_2$O$_3$ nanocomposites. *J Eur Ceram Soc* 1998;**18**:209–19.
6. Nawa M, Nakamoto S, Bamba N, Sekino T, Niihara K. Tough and strong Ce-TZP/alumina nanocomposites doped with titania. *Ceram Int* 1998;**24**:497–506.
7. Benzaid R, Chevalier J, Saâdaoui M, Fantozzi G, Nawa M, Diaz L, et al. Fracture toughness, strength and slow crack growth in a ceria stabilized zirconia–alumina nanocomposite for medical applications. *Biomaterials* 2008;**29**:3636–41.
8. Ban S, Bawa M. Application of zirconia/alumina composite to all ceramic crown. *Dent Mater J* 2005;**24**:70.
9. Ban S, Nawa M, Suehiro Y, Nakanishi H. Mechanical properties of zirconia/alumina nano-composite after soaking in various water-based conditions. *Key Eng Mater* 2006;**309–311**:1219–22.
10. Ban S, Sato H, Suehiro Y, Nakanishi H, Nawa M. Biaxial flexure strength and low temperature degradation of Ce-TZP/Al$_2$O$_3$ nanocomposite and Y-TZP as dental restoratives. *Biomed Mater Res Part B: Appl Biomater* 2008;**87B**:492–8.
11. Tanaka K, Tamura J, Kawanabe K, Nawa M, Oka M, Uchida M. Ce-TZP/Al$_2$O$_3$ nanocomposites as a bearing material in total joint replacement. *J Biomed Mater Res* 2002;**63**:262–70.
12. Tanaka K, Tamura J, Kawanabe K, Nawa M, Uchida M, Kokubo T, et al. Phase stability after aging and its influence on pin-on-disk wear properties of Ce-TZP/Al$_2$O$_3$ nanocomposite and conventional Y-TZP. *J Biomed Mater Res A* 2003;**67**:200–7.
13. Toraya H, Yoshimura M, Somiya S. Calibration curve for quantitative analysis of the monoclinic–tetragonal ZrO$_2$ system by X-ray diffraction. *J Am Ceram Soc* 1984;**67**:C119–21.
14. Chevalier J, Olagnon C, Fantozzi G. Study of the residual stress field around Vickers indentation in a 3Y-TZP. *J Mater Sci* 1996;**31**:2711–7.

15. de Armas Sancho Z, Jiménez-Piqué E, Mestra A, Anglada M. Contact damage in artificially aged 3Y-TZP. In: *IOP Conf. Series: Materials Science and Engineering, vol. 5*. 2009. p. 012013.

16. Lawn BR. Indentation of ceramics with spheres: a century after hertz. *J Am Ceram Soc* 1998;**81**:1977–94.

17. Tabor D. *The Hardness of Metals*. 1st ed. London, United Kingdom: Oxford University Press; 1951.

18. Herbert EG, Pharr GM, Oliver WC, Lucas BN, Hay JL. On the measurement of stress–strain curves by spherical indentation. *Thin Solid Films* 2001;**398–399**:331–5.

19. Oliver WC, Pharr GM. An improved technique for determining hardness and elastic modulus using load and displacement sensing indentation experiments. *J Mater Res* 1992;**7**:1564–83.

20. Katagiri G, Ishida H, Ishitani A, Masaki T. Direct determination by Raman microprobe of the transformation zone size in Y_2O_3 containing tetragonal ZrO$_2$ polycrystals. In: Somiya S, Yamamoto N, Yanagida H, editors. *Science and Technology of Zirconia III*. Westerville, OH: American Ceramic Society; 1988. p. 537–44.

21. Muñoz Tabares A, Anglada M. Quantification of monoclinic phase in 3Y-TZP by Raman spectroscopy. *J Am Ceram Soc* 2010;**93**:1790–5.

22. Muñoz Tabares A, Jiménez-Piqué, Anglada M. Subsurface evaluation of hydrothermal degradation of zirconia. *Acta Mater* 2011;**59**:473–84.

23. Marro FG, Valle J, Mestra A, Anglada M. Surface modification of 3Y-TZP with cerium oxide. *J Eur Ceram Soc* 2011;**31**:331–8.

24. Rauchs G, Fett T, Munz D, Oberacker R. Tetragonal to monoclinic phase transformation in CeO_2-stabilized zirconia under uniaxial loading. *J Eur Ceram Soc* 2001;**21**:2229–41.

25. Janssen M, Zuidema J, Wanhill R. *Fracture Mechanics*. 2nd ed. Spon Press; 2004.